Spin currents with unusual spin orientations in noncollinear Weyl antiferromagnetic math xmlns="http://www.w3.org/1998/Math/MathML">mrow>msub>mi>Mn/mi>mn>3/mn>/msub>mi>Sn/mi>/mrow>/math>

Xinhao Wang, Mohammad Tomal Hossain, T. R. Thapaliya, Durga Khadka, Sergi Lendinez, Hang Chen, Matthew F. Doty, M. Benjamin Jungfleisch, S. X. Huang, Xin Fan, and John Q. Xiao

Phys. Rev. Materials **7**, 034404 — Published 10 March 2023

DOI: 10.1103/PhysRevMaterials.7.034404

Spin currents with unusual spin orientations in noncollinear Weyl antiferromagnetic Mn_3Sn

Xinhao Wang[1,*], Mohammad Tomal Hossain[1], T. R. Thapaliya[2], Durga Khadka[2], Sergi Lendinez[1], Hang Chen[1], Matthew F. Doty[3], M. Benjamin Jungfleisch[1], S. X. Huang[2], Xin Fan[4], John Q. Xiao[1,†]

1 Department of Physics and Astronomy, University of Delaware, Newark, Delaware 19716, United States
2 Department of Physics, University of Miami, Coral Gables, FL, 33146, USA
3 Department of Materials Science and Engineering, University of Delaware, Newark, Delaware 19716, United States
4 Department of Physics and Astronomy, University of Denver, Denver, Colorado 80210, USA

† Corresponding authors: jqx@udel.edu

Abstract

There are intensive efforts to search for mechanisms that lead to spin-orbit torque with unusual spin orientation, particularly out-of-plane spin orientation which can efficiently switch perpendicular magnetizations. Such a phenomenon has been observed in materials with low structural symmetry, ferromagnetic materials, and antiferromagnets with non-collinear spin structures. Here, we demonstrate the observation of, in addition to out-of-plane spin orientation, spin orientation along the charge current direction in Mn_3Sn, a noncollinear antiferromagnet and Weyl semimetal. The mechanism arises from non-collinear spin structure with spin-orbit coupling and it can be viewed as spin rotation around the octupole moment, the lowest order of cluster multipole moment pertaining to Mn_3Sn crystal group.

The heart of spin-orbitronics aims to generate spin current from charge current, which enables electrical control of magnetization. Conventional spin-orbit effects, such as the spin Hall effect in heavy metals (HMs), generate spin currents with spin orientation perpendicular to both spin current and applied charge current directions [1,2]. Such a spin current can be described by a spin-conductivity sensor of σ_{zx}^{y}, where *x* and *y* define a film plane, the first and second subscripts defines the spin current and charge current directions, respectively, and the superscript defines the spin orientation. Motivated by applications to switch perpendicular magnetization without a bias field, researches are focusing on searching for materials that have sizable σ_{zx}^{z}, i.e., out-of-plane spin orientation [3]. It is also interesting to find materials with nonzero σ_{zx}^{x}. For example, in WTe_2, since the absence of its mirror symmetry in the *xy* plane, an applied electric current within that mirror plane can generate a spin current described by σ_{zx}^{x} [3]. It has also been shown that in a simple perpendicularly magnetized metal film, where magnetization breaks mirror symmetries, a similar spin current can be generated, i.e., $\sigma_{zx}^{x} \neq 0$ [4]. This effect was referred to as spin rotation since the x-polarized spins can be viewed as a result of y-polarized spins precess around the perpendicular magnetization.

Very recently, it has been shown that Mn_3Sn, a non-collinear antiferromagnet [5,6] and a Weyl semimetal [7,8], also exhibits unique charge-to-spin conversion, dubbed as the magnetic spin Hall effect [9]. Mn atoms in Mn_3Sn form a Kagome lattice with their spins 120^o degree apart from their nearest neighbors. This leads to cluster magnetic multipole (CMP) moment that, similar to a simple magnetic moment, breaks time reversal symmetry and mirror symmetries [10]. It has been experimentally and theoretically demonstrated that the Mn_3Sn can generate spin currents similar to that in

ferromagnet [9,11,12]. For example, if the CMP moment lies in the film plane, one would observe spin current described by σ_{zx}^{z}, which is also able to switch a perpendicular magnetization without a bias field [11]. In this paper, we report that, in addition to σ_{zx}^{z}, σ_{zx}^{x} also exists in Mn_3Sn with CMP moment lying in the film plane, which has not been predicted in theory, nor has been observed experimentally. The results are confirmed by magneto-optical Kerr effect (MOKE) spin orbit torque magnetometer and spin torque ferromagnetic resonance (ST-FMR) [13–16]. We attribute the experimental observation to the SHE effect with spin rotation in noncolinear AFM. In other words, conventional SHE generates spin orientation transverse to the charge current direction rotates around the octupole moment, the lowest order of CMP pertaining to Mn_3Sn crystal group, which generates spin orientation in both parallel and perpendicular to the applied electric current direction.

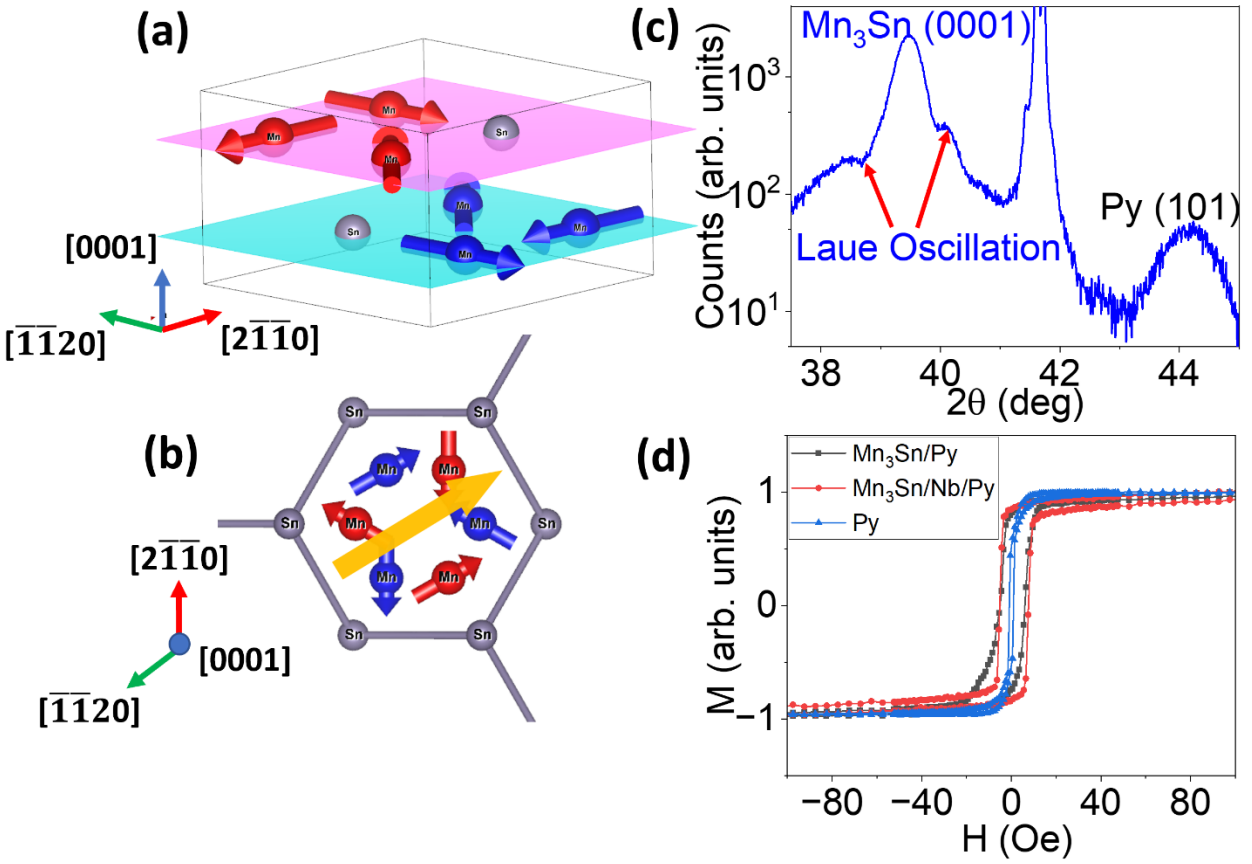

Figure 1 (a) *The Mn moment (red and blue arrows) lies in the ab plane with an ABAB stacking sequence. Red and blue sphere represent the Mn atom on z=0 and z=1/2, respectively.* ***(b)*** *Six moments from the Mn atoms (red & blue arrows) forms the cluster magnetic octupole (yellow arrow).* ***(c)*** *The XRD result of the //Al_2O_3/Pt(1.5nm)/Mn_3Sn(30nm)/Nb(2nm)/Py(10nm)/SiO_2 sample shows Mn_3Sn is c-axis [0001] oriented with crystal and magnetic structure shown in (a).****(d)*** *The hysteresis loops of Mn_3Sn(30nm)/Py(10nm) (black curve), Mn_3Sn(30nm)/Nb(2nm)/Py(10nm) films (red curve), and Py(30nm) (blue curve).*

Methods

Sample growth, fabrication, and characterization

The multilayer films were grown in 5.3 mTorr argon gas by DC sputtering in a high-vacuum magnetron sputtering system with a base pressure better than 5×10^{-8} torr. The Pt seed layer was grown on Al_2O_3 (0001) substrate at substrate temperature (T_S) of 500 ºC, followed by annealing at the same temperature for 3 hours. (0001) $Mn_{3+x}Sn_{1-x}$ compositional wedge films along 2" wafer were then co-sputtered from Mn and Sn targets at $T_S \approx 300\ ^{o}\mathrm{C}$ [17] without further annealing. $Ni_{81}Ni_{19}$ (Py) or Nb/Py were deposited at room temperature, forming $Mn_{3+x}Sn_{1-x}$(30nm)/Py(10nm) and $Mn_{3+x}Sn_{1-x}$(30nm)/Nb(2nm)/Py(10nm) heterostructure. The insertion of Nb layer is used to isolate the direct coupling between Mn_3Sn and Py and to investigate the interface effect. The thickness of Py and Nb were calibrated with X-ray reflectivity. All ST-FMR and MOKE devices were fabrication by patterning the film using laser writer (Heidelberg MLA100) lithography following with ion milling (IntlVAC Nanoquest). Then 3 nm Ti/ 200nm Au was deposited with magnetron sputtering as electrodes.

Extraction of the saturation magnetization and switching field of Mn_3Sn CMP using spin-pumping technique

The spin-pumping experiment was used to measure the saturation magnetization of the Py layer in our Mn_3Sn(30nm)/Nb(2nm)/Py(10nm) and Mn_3Sn(30nm)/Py(10nm) samples. During the measurement, we measure the rectifying voltage as a function of the field at different frequencies from 8 GHz to 15 GHz. The input microwave power is set at 25 dB. Since the frequency dependence of the resonance field B_r could be fitted by the Kittel formula $2\pi f = \gamma\sqrt{B_{\mathrm{r}}(B_{\mathrm{r}} + \mu_0 M_{\mathrm{s}})}$, where μ_0 is the magnetic constant and γ is the gyromagnetic constant (the ratio of the magnetic dipole moment to the angular momentum) [18]. We could extract from the fitting that $\mu_0 M_{\mathrm{s}} = 0.45$ T.

Furthermore, since the different behaviors of the symmetric components in spin-pumping experiment at positive and negative fields will indicate if the CMP is switched at the resonance field [9]. We can determine the switching field of octupole moment in our Mn_3Sn films. If the symmetric components in positive and negative fields have the opposite sign (similar to the behavior in conventional Py/Pt sample), this means the Mn_3Sn CMP does not switch at the resonance field, otherwise the sign would have changed. From the data measured at different frequency, we can estimate the switching field of Mn_3Sn in the present device is about 0.85 kOe which is larger than the applied magnetic field range (0 to 0.8 kOe) during our MOKE and STT-FMR measurements. This conclusion is consistent with our previous discussion on Figure 3. Both of them indicate that within the applied magnetic field range (0 to 0.8 kOe) during the MOKE and STT-FMR measurements, the Mn_3Sn CMP direction is not aligned in the field direction.

ST-FMR measurement

During the ST-FMR experiment, a rf current i_{rf} at 5GHz with power of 10 dBm was sent through the sample strip along the *x-axis*. The external magnetic field was applied in the *x-y* plane with an angle θ away from *x*-axis and swept from 0 to 800 Oe for driving the ferromagnetic layer Py through its resonance conditions. The rf current amplitude is modulated at 1.3 kHz and the lock-in amplifier is used for signal detection.

From Eq.(10) and Eq.(11) we learn that the V_{Sym} and V_{Asym} are proportional to in-plane torque $\tau_{\parallel}$ and out-of-plane torque $\tau_{\perp}$ which can be expressed as

$$V_{\mathrm{Sym}} = -\frac{I_{\mathrm{rf}}}{2}\left(\frac{dR}{d\theta}\right)\frac{1}{\alpha(2\mu_0 H_{\mathrm{R}} + \mu_0 M_{\mathrm{eff}})}\tau_{\parallel} \quad (12)$$

$$V_{Asym} = -\frac{I_{\mathrm{rf}}}{2}\left(\frac{dR}{d\theta}\right)\frac{\sqrt{1+\frac{M_{\mathrm{eff}}}{H_{\mathrm{R}}}}}{\alpha(2\mu_0 H_{\mathrm{R}} + \mu_0 M_{\mathrm{eff}})}\tau_{\perp} \quad (13)$$

where I_{rf} is the microwave current, R is the device resistance as a function of in-plane H field direction θ due to the AMR of Py, α is the Gibert damping coefficient, M_{eff} is the effective magnetization and H_{R} is the resonance field. If we assuming the τ_{FL}^{y} is dominated by the Oersted field, the SHA of the Mn_3Sn can be expressed as:

$$\theta_{zx}^{x} = \frac{\tau_{\mathrm{x,DL}}}{\tau_{\mathrm{y,FL}}}\frac{\mathrm{e}\mu_0 M_{\mathrm{s}} t_{\mathrm{Py}} t_{\mathrm{Mn_3Sn}}}{\hbar} \quad (14)$$

$$\theta_{zx}^{y} = \frac{\tau_{\mathrm{y,DL}}}{\tau_{\mathrm{y,FL}}}\frac{\mathrm{e}\mu_0 M_{\mathrm{s}} t_{\mathrm{Py}} t_{\mathrm{Mn_3Sn}}}{\hbar} \quad (15)$$

$$\theta_{zx}^{z} = \frac{\tau_{\mathrm{z,DL}}}{\tau_{\mathrm{y,FL}}}\frac{\mathrm{e}\mu_0 M_{\mathrm{s}} t_{\mathrm{Py}} t_{\mathrm{Mn_3Sn}}}{\hbar} \quad (16)$$

where t_{Py} and $t_{\mathrm{Mn_3Sn}}$ are the thickness of the Py and Mn_3Sn layers. With Eqs.(12-16), we can calculate the SHA of Mn_3Sn without knowing the I_{rf} and $\frac{dR}{d\theta}$ since we only use the ratio between $\tau_{\parallel}$ and $\tau_{\perp}$ terms. $M_{\mathrm{eff}} = 5.5 \times 10^5$ A/m which is extracted from the VSM result.

MOKE measurement

During the MOKE measurement, we were using the 780-nm femtosecond pulsed laser (Toptica FemtoFiber pro NIR) with a repetition rate of 80 MHz as our beam source. The laser beam focused spot size is ~2.95 μm^2. 10 mA (RMS) *Sin* function wave AC current at 1.777 kHz was passing through the sample during the measurement. For more information on our MOKE system, please refer to [19] in which detailed describe our MOKE system.

One of advantages of using polar MOKE to determine spin-orbit fields is that the out-of-plane Oersted field can be determined which can be further used to quantify the effective fields of spin orbit torques, allowing the accurate determination of the spin Hall angel of θ_{xz}^{x} and θ_{xz}^{y} [13]. By plot the symmetric contribution, $\Delta\psi(+\boldsymbol{m}) + \Delta\psi(-\boldsymbol{m})$ and antisymmetric contribution, $\Delta\psi(+\boldsymbol{m}) - \Delta\psi(-\boldsymbol{m})$, we can

determine the out-of-plane Oersted field and h_{SOT}, respectively. The linescan $\Delta\psi(+\boldsymbol{m}) + \Delta\psi(-\boldsymbol{m})$ across the width (transverse to the current) of the sample is due to the out-of-plane Oersted field $h_{z,Oe}\ since\ \Delta\psi(+m_x) + \Delta\psi(-m_x) = \frac{2\alpha_{\mathrm{Polar}}\langle h_{\mathrm{z,Oe}}\rangle}{H_{\mathrm{ext}}+H_{\mathrm{anis}}+M_S-H_{\mathrm{anis}\perp}}$,where $\langle h_{\mathrm{z,Oe}}\rangle$ is the average field in the region illuminated by the laser. The out-of-plane Oersted field can be calculated following Ampere's Law, $h_{\mathrm{z,Oe}} = \frac{I}{2\pi w} ln \frac{y}{w-y}$, where w is the width of the sample strip [13]. The antisymmetric contribution is given by $\Delta\psi(+\boldsymbol{m}) - \Delta\psi(-\boldsymbol{m}) = \frac{2\alpha_{\mathrm{Polar}}\, h_{DL}^{y}}{H_{\mathrm{ext}}+H_{\mathrm{a}}+M_{\mathrm{S}}-H_{\mathrm{a}\perp}}$. Since the current is uniform distributed across the Mn_3Sn layer, the effect field h_{DL}^{y} from the SHE of the Mn_3Sn is also uniform across the sample. We extract the $\mu_0 h_{SOT} = 0.0106 \pm 0.003$mT at a 10mA current through the 40 μm wide sample strip. Mn_3Sn has resistivity about 250 μΩ•cm, Py has resistivity about 40 μΩ•cm, thickness of Mn_3Sn is 30nm while it is 10 nm for Py. Therefore, R_{Mn3Sn} is about twice of R_{Py} and approximately 30% of the current flows through Mn_3Sn via parallel resistor model, yielding a current density in the Mn_3Sn $j_{Mn_3Sn} = \frac{10\ mA*0.33}{30nm*40\mu m} = 2.77 * 10^9 A/m^2$. If we assume all of the antidamping-like torque is dure to the SHA in the Mn_3Sn layer, we determine a spin Hall angle $\theta_{Mn_3Sn,y} = 0.042 \pm 0.012$ (using the formula $\theta_{\mathrm{SH}} = (2e/\hbar)\mu_0 h_{\mathrm{z,SO}} M_{\mathrm{s}} d_{\mathrm{Py}}/j_{\mathrm{Pt}}$).

According to the Eq. (3), the quadratic MOKE signal as a function of the applied magnetic field along the current direction follows $1/H_{ext}$ dependence and the asymmetry on the positive and negative region represent the damping-like torque from the z-polarized spin current h_{DL}^{z}. In practice, the difference in fitting parameter A at the negative and positive field region represent the τ_{DL}^{Z}. For example, in Figure S3, the values of $A(+m_x) + A(-m_x)$ and $A(+m_x) - A(-m_x)$ are -0.0031 and -0.00046, respectively. This translates to h_{FL}^{y} being $\frac{0.0031}{0.00046} = 6.7$ times larger than τ_{DL}^{Z}. For Py/Pt reference sample, $A(+m_x) - A(-m_x)$ does not exist, due to the absence of τ_{DL}^{Z}.

RESULTS

Mn_3Sn, which is a Weyl semimetal and non-collinear AFM, has a hexagonal structure with lattice constants a=0.567 nm and c= 0.453 nm (Figure 1 (a)) [17]. The broken time-reversal symmetry together with spin orbit coupling leads to Weyl semimetal properties and AHE [20]. The intrinsic AHE, in modern AHE formulism, is directly related to the Berry curvature, which characterizes the topological entanglement between conduction and valence bands and is equivalent to a magnetic field in the momentum space [20]. Most recently, both theoretical calculation [10] and experiment [21]show that the Berry curvature and the octupole moment are in the same direction and rotate together with triangular spins in the *ab* plane [21](Figure 1 (b)).

The $Mn_{3+x}Sn_{1-x}$(30nm)/Py(10nm) and $Mn_{3+x}Sn_{1-x}$(30nm)/Nb(2nm)/Py(10nm) multilayer films were grown on (0001) Al_2O_3 substrate by DC sputtering system(see "methods") [17]. The results presented here are from samples with x ~ 0.05 (Hereafter we will use Mn_3Sn to represent this composition). The Mn_3Sn film used in this study has also been well characterized to be single crystal and form the same inverse triangular spin structure as bulk samples in our previous study [17,22](see "supplementary information"). The insertion of Nb layer is used to isolate the direct coupling between Mn_3Sn and Py and to investigate the interface effect. The compositions of Mn_3Sn films were measured on 150 nm films by energy dispersive spectrometer (EDS) in a scanning electron microscope (SEM). As shown in X-ray diffraction

(XRD) (Figure1(c)), we have achieved high quality c-axis oriented Mn_3Sn films, evident from the two Laue oscillations. The room temperature hysteresis loops of Mn_3Sn/Py and Mn_3Sn/Nb/Py films, as well as a reference sample of single Py layer on Si wafer are shown in Figure1 (d). Both Mn_3Sn samples show no observable hysteresis shift and slightly increased coercivity of about 4 Oe. This small increase in coercivity is unlikely due to exchange coupling between Mn_3Sn and Py since the insertion of Nb layer would suppress it. The small increase in coercivity is probably due to roughness of Mn_3Sn and Mn_3Sn/Nb. This result is consistent with previous study [23] that shows almost no exchange coupling between Mn_3Sn(40nm) and Py(5nm) bilayers at room temperature.

Considering a perpendicular spin current (z-axis) consisting of an arbitrary spin polarization, there are total 6 possible effective spin-orbit torques (SOTs) components of τ_{DL}^{σ} and τ_{FL}^{σ} and related effect fields of h_{DL}^{σ} and h_{FL}^{σ}, where all superscripts σ= *x*, *y*, *z* represents spin orientation, and DL and FL stand for damping-like torque and field-like torque, respectively. For the conventional SHE, only τ_{DL}^{y} and τ_{FL}^{y} (h_{DL}^{y} and h_{FL}^{y}) exist. We first employ MOKE measurement to characterize the SOTs and associated spin orientations. MOKE directly measures the torque-induced moment rotation instead of second-order rectifying voltage from changing resistance which is more susceptible to other nonlinear or thermal effects [13,16,24]. The polarization angle $\psi(m)$ of the normal incident light with linear polarization is rotated by the magnetization and can be written as:

$$\psi(\boldsymbol{m}) = \alpha_{\text{Polar}}\, m_z + \beta_{\text{Quadratic}}\, m_{\text{x}} m_{\text{y}} + \cdots \qquad (1)$$

where α_{Polar} and $\beta_{\text{Quadratic}}$ are the coefficients for the polar MOKE and quadratic MOKE responses, respectively. For films with both magnetization and current along the *x*-axis, the conventional SHE leads to the effective fields h_{FL}^{y} and h_{DL}^{y} in the *y*-axis and *z*-axis, respectively (Figure 2(a)), which can be characterized by measuring azimuthal angles ϕ_M and the polar angle θ_M, respectively.

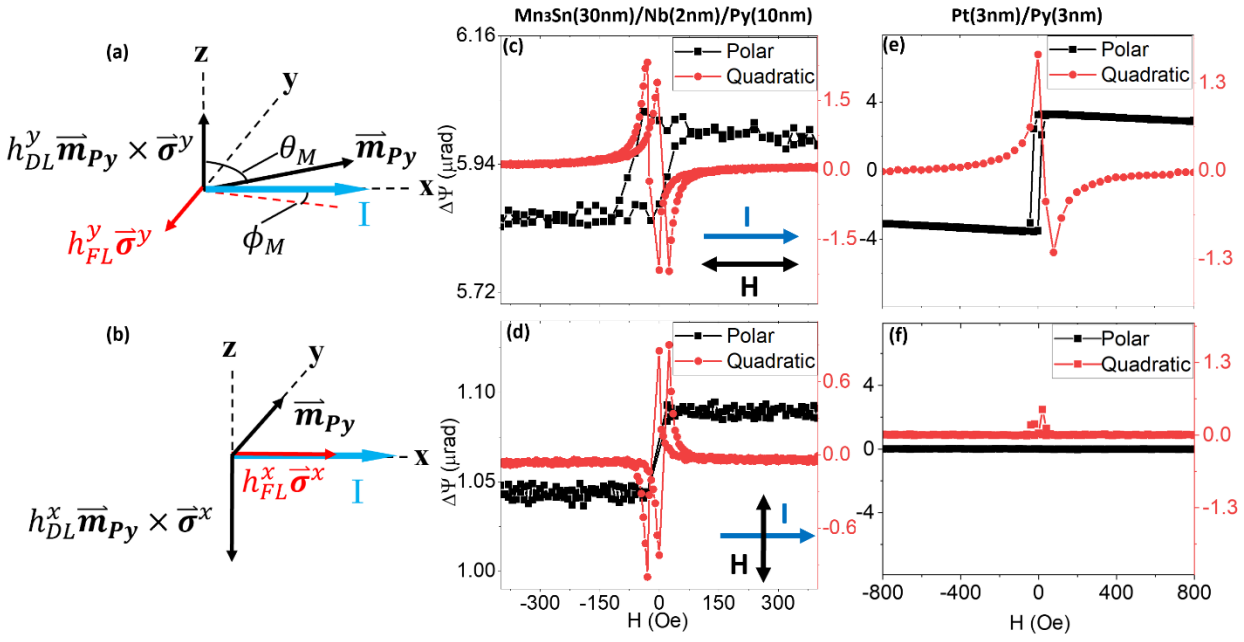

Figure 2 (a),(b)*Illustration of the effective field of SOTs, magnetization, and current direction in two measurements , the current is flowing along the x-axis while the external field is applied parallel (a) and perpendicular (b) to the current direction.* ***(c)-(f)*** *The quadratic MOKE (red) and polar MOKE (black)*

results with the external field ((c),(e)) parallel to the current direction and ((d),(f)) perpendicular to the current direction for Mn_3Sn/Nb/Py (middle column) and Pt/Py (right column).

The quadratic MOKE, which is purely related to the in-plane effective field, can be independently measured using circularly polarized light which does not respond to m_z [13]. In addition, the effect of h_{FL}^{y} will disappear if one aligns the magnetization along the *y*-axis. In this geometry one would see the effect of h_{FL}^{x}, if it exists. Using the small angle approximation and Jones matrices, we can determine the spin-orbit torque induced polarization change as:

$$\Delta\psi(\boldsymbol{m}) = -\beta_{\text{Quadratic}}\,\Delta\phi_{\text{M}} \quad (2)$$

where, for the magnetic field (H_{ext}) applied along the *x*-axis:

$$\Delta\phi_M = \frac{h_{FL}^{y} + h_{DL}^{z} + h_{y,Oe}}{H_{ext} + H_a + h_{FL}^{x}} \quad (3)$$

where H_a is the in-plane anisotropy field and $h_{y,Oe}$ is the in-plane Oersted field. The Oersted field $h_{y,Oe}$ is opposite on the top and bottom surfaces of the Py layer. Since the Py layer thickness (10nm) is smaller than the penetration depth of the laser in Py, this term is negligible in both Eqs.(3) and (6). Because h_{FL}^{y} and h_{DL}^{z} is antisymmetric and symmetric with respect to the magnetization (external field), respectively, the h_{FL}^{y} and h_{DL}^{z} can be determined using:

$$\Delta\phi(+m_x) + \Delta\phi(-m_x) = \frac{2h_{FL}^{y}}{H_{ext}+H_a+h_{FL}^{x}} \quad (4)$$

and

$$\Delta\phi(+m_x) - \Delta\phi(-m_x) = \frac{2h_{DL}^{z}}{H_{ext}+H_a+h_{FL}^{x}} \quad (5)$$

If we apply the magnetic field to align the magnetization along the *y*-axis, we then have:

$$\Delta\phi_M = \frac{h_{FL}^{x}}{H_{ext} + H_a + h_{FL}^{y} + h_{DL}^{z} + h_{y,Oe}} \quad (6)$$

For soft NiFe alloys, both h_{FL} and H_a are negligible compared with the external field, the quadratic MOKE will show $1/H_{ext}$ dependence according to Eq.(3) and (6).

The polar MOKE signal can be determined by using linear polarized light with 45° between the polarization and magnetization, at which quadratic MOKE disappear [13]. For an external field along the *x*-axis we have

$$\Delta\psi(\boldsymbol{m}) = \alpha_{\text{Polar}}\,\Delta\theta_{\text{M}} = \alpha_{\text{Polar}}\,\frac{h_{DL}^{y} + h_{z,Oe}}{H_{\text{ext}} + H_{\text{a}} + M_{\text{S}} - H_{\text{a}\perp}} \quad (7)$$

where $h_{z,Oe}$ is the out-of-plane Oersted field, M_{S} is the saturation magnetization, and H_a and $H_{\text{a}\perp}$ are the in-plane anisotropy field and out-of-plane anisotropy. The saturation magnetization (M_S) for Py film is about 0.45T as extracted from spin-pumping experiment(see "methods"), which is far larger than all other field terms. Consequently, Eq. (7) leads to a hysteresis loop-like behavior as shown in black curves in

Figure 2. One can also conveniently separate the $h_{Dl}^{x}$and h_{DL}^{y} by applying the external field in *x* or *y* direction, respectively.

The results for Mn_3Sn/Nb/Py (Mn_3Sn/Py shows similar results) and a reference Pt/Py sample are shown in Figure 2 with current along the x-axis ($[01\bar{1}0]$ direction of Mn_3Sn film) which is 30 degree to the Mn_3Sn CMP direction of $[11\bar{2}0]$. From the spin-pumping measurement (see "methods") and ST-FMR measurement result (Figure 3), we conclude that the CMP direction is not aligned within the applied magnetic field range (0 to 0.8 kOe) during the MOKE measurements. Figure 2(c), (e) and (d),(f) show results measured with the applied field along the *x*-axis, and *y*-axis, respectively. Figure 2(c) shows similar behavior with FM/HM, indicating the spin orientation is along the y-axis. The results in Figure 2(d) compared to those of Pt/Py (Fig. 2(f)) clearly demonstrate the existence of τ^x component in Mn_3Sn/Nb/Py. By analyzing the quadratic MOKE (red curves) using Eqs. (4) and (5), we can also detect τ^z in additional to conventional τ^y component. In another word, we have observed all 3 spin orientations along *x*, *y*, and *z* in charge-induce spin current. From these results, we can determine the spin Hall angle of $\theta_{zx}^{x} = -0.014 \pm 0.004$ and $\theta_{zx}^{y} = 0.042 \pm 0.012$ for spin currents with spin orientation in *x*- and *y*-directions, respectively (see "methods"). The value for θ_{zx}^{y} is consistent with the previous reported value extracted from spin pumping experiment [25]. We can further determine the torque ratio of $\tau_{FL}^{x}: \tau_{FL}^{y}: \tau_{DL}^{z} = 0.3 \pm 0.12: 1: 0.29 \pm 0.14$. and $\tau_{DL}^{x}: \tau_{DL}^{y} = 0.37 \pm 0.04$. These values indicate that the spin current with spin orientation along the x-axis is about 30% of spin current with spin orientation along the y-axis. These results are summarized in Table 1.

Table 1: *The torque ratio extracted from ST-FMR and MOKE measurements for Mn_3Sn/Py and Mn_3Sn/Nb/Py films.*

		$\boldsymbol{\tau_{FL}^{x}: \tau_{FL}^{y}: \tau_{DL}^{z}}$	$\boldsymbol{\tau_{DL}^{x}: \tau_{DL}^{y}: \tau_{FL}^{z}}$
MOKE	Mn_3Sn/Py	-0.27±0.11: 1: 0.25±0.12	-0.33±0.03:1:NA
	Mn_3Sn/Nb/Py	-0.30±0.12: 1: 0.29±0.14	-0.37±0.04:1:NA
ST-FMR	Mn_3Sn/Py	-0.009: 1: -0.035	-0.26:1:1.63
	Mn_3Sn/Nb/Py	0.04: 1: -0.0096	-0.37:1:2.32

In order to conform the observed unconventional spin orientations, we also performed ST-FMR experiment. In the experiment, a rf current i_{rf} was sent through the sample strip along the *x-axis*. The external magnetic field was applied in the *x-y* plane with an angle θ away from *x*-axis. We should note that τ^x, τ^y and τ^z shows different angular dependences. To be specific, τ^x has a $\sin\theta$ dependence, τ^y has a $\cos\theta$ dependence while τ^z is independent of θ. The rectifying voltage V_{dc} contains symmetric V_{Sym} and antisymmetric V_{Asym} contributions, which are proportional to in-plane torque $\boldsymbol{\tau}_{\parallel} R_{AMR}$ and out-of-plane torque $\boldsymbol{\tau}_{\perp} R_{AMR}$, respectively. With R_{AMR} showing $\sin(2\theta)$ dependence, and each $\boldsymbol{\tau}_{\parallel}$ and $\boldsymbol{\tau}_{\perp}$ is composed of three effective torques we mentioned earlier. The general form of the V_{Sym} and V_{Asym} for spin orientation in an arbitrary direction is [26]:

$$V_{\mathrm{Sym}}(\theta) \propto \sin(2\theta)\left(\tau_{DL}^{x}\sin(\theta) + \tau_{DL}^{y}\cos(\theta) + \tau_{FL}^{z}\right) \quad (10)$$

$$V_{\text{Asym}}(\theta) \propto \sin(2\theta)\left(\tau_{FL}^{x}\sin(\theta) + \tau_{FL}^{y}\cos(\theta) + \tau_{DL}^{z}\right) \quad (11)$$

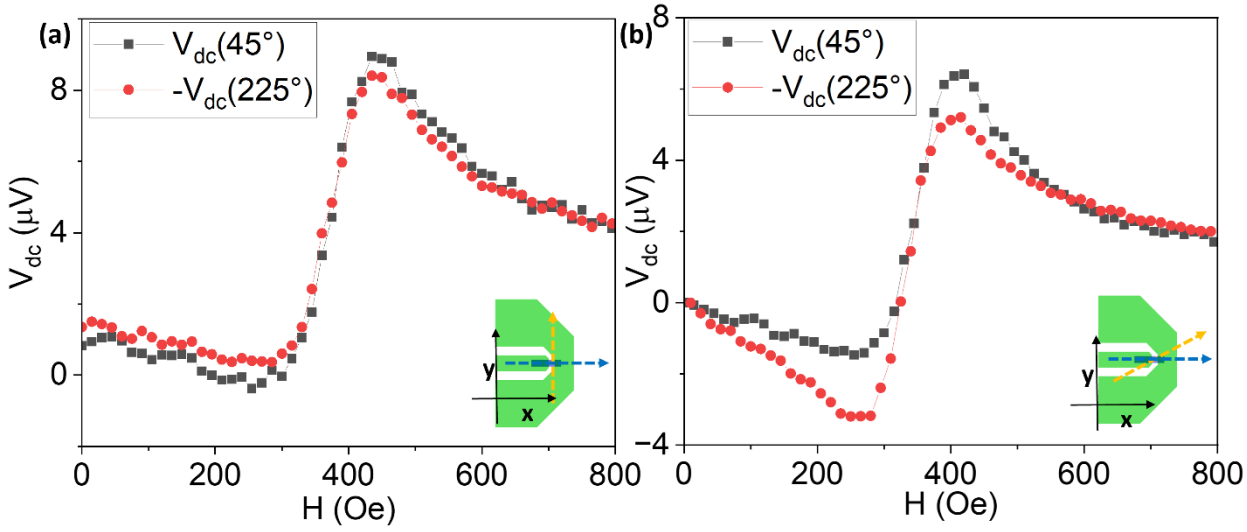

Figure 3 *ST-FMR spectra. V_{dc} for the Mn_3Sn/Py device with the Py magnetization oriented at 45° and 225° relative to the current direction (blue arrow). The result of (a) and (b) were obtained from the octupole moment of Mn_3Sn(yellow arrow) pointing to (a) perpendicular and (b) 30° to the current direction. The rf current was at 5GHz with power of 10 dBm.*

In addition to confirming spin orientations along the x- and z-axis, we also investigate their relationship with the octupole moment in Mn_3Sn. In the conventional case, since only τ_{DL}^{y} and τ_{FL}^{y} exist, when m_{Py} is inverted in *x-y* plane by the magnetic field, V_{dc} must remain the exact same amplitude with an opposite sign. As shown in Figure 3(a), when the current is flowing along the $[1\bar{1}00]$ direction of the Mn_3Sn film which is perpendicular to the octupole moment ($[11\bar{2}0]$) [22], we observe that $V_{dc}(45°)$ and $V_{dc}(225°)$ have the same amplitude but opposite phase, indicating only τ_{DL}^{y} and τ_{FL}^{y} exist just like that from a heavy metal. This result is consistent with the pervious theoretical and experimental results [11,12]. However, when we pass the current along the $[01\bar{1}0]$ direction, which forms 30° with respect the octupole moment (Figure 3(b)), the amplitudes for $V_{dc}(45°)$ and $V_{dc}(225°)$ are clearly different, suggesting the existence of τ^{z}. These results further imply that spin orientations along z- direction may arise from the spin rotation around the octupole moment, i.e. spin orientation in y-direction arising from SHE rotates around the octupole to introduce spin orientations in other two directions. It is also known that the sign of SHA of Mn_3Sn reverses if Mn Moments are reversed, which would change the sign of $-V_{dc}(225°)$ [9] . We therefore conclude the Mn moment in our samples is not switched in the field range used in our study.

The torque components can be further evaluated quantitatively with the angle-dependent ST-FMR results. Figure 4 shows the angle dependent ST-FMR signals with the microwave current applied 30 degree from the octupole (same geometry in Figure 3 (b) and MOKE measurements). The V_{sym} and V_{Asym} curves are fitted with only τ^{y} terms as in conventional case (red curves) and unconventional case with all$\tau^{x}, \tau^{y}, and\ \tau^{z}$ toque terms using Eq. (10) and (11). While the fittings show no obvious difference in V_{Asym}, V_{Sym} curves can only be fitted with additional torque terms of τ_{DL}^{x} and τ_{FL}^{z} (blue curve). We can further determine the ratio between τ_{DL}^{x}, τ_{DL}^{y} and τ_{FL}^{z} which is consistent with the MOKE result (Table 1). Furthermore, by assuming that the conventional field-like torque is negligible compared to Oersted field which contributes mostly to the τ_{FL}^{y} [26], we can also extract the spin Hall angle of $\theta_{zx}^{x} = -0.013$, $\theta_{zx}^{y} = 0.053$, and $\theta_{zx}^{z} = -0.007$ for spin currents with spin orientation in *x*-, *y*- and z- directions, respectively

(see "methods"). The results of $\tau_{FL}^{x}:\tau_{FL}^{y}:\tau_{DL}^{Z}$, on the other hand, are very different from those determined from MOKE experiments.

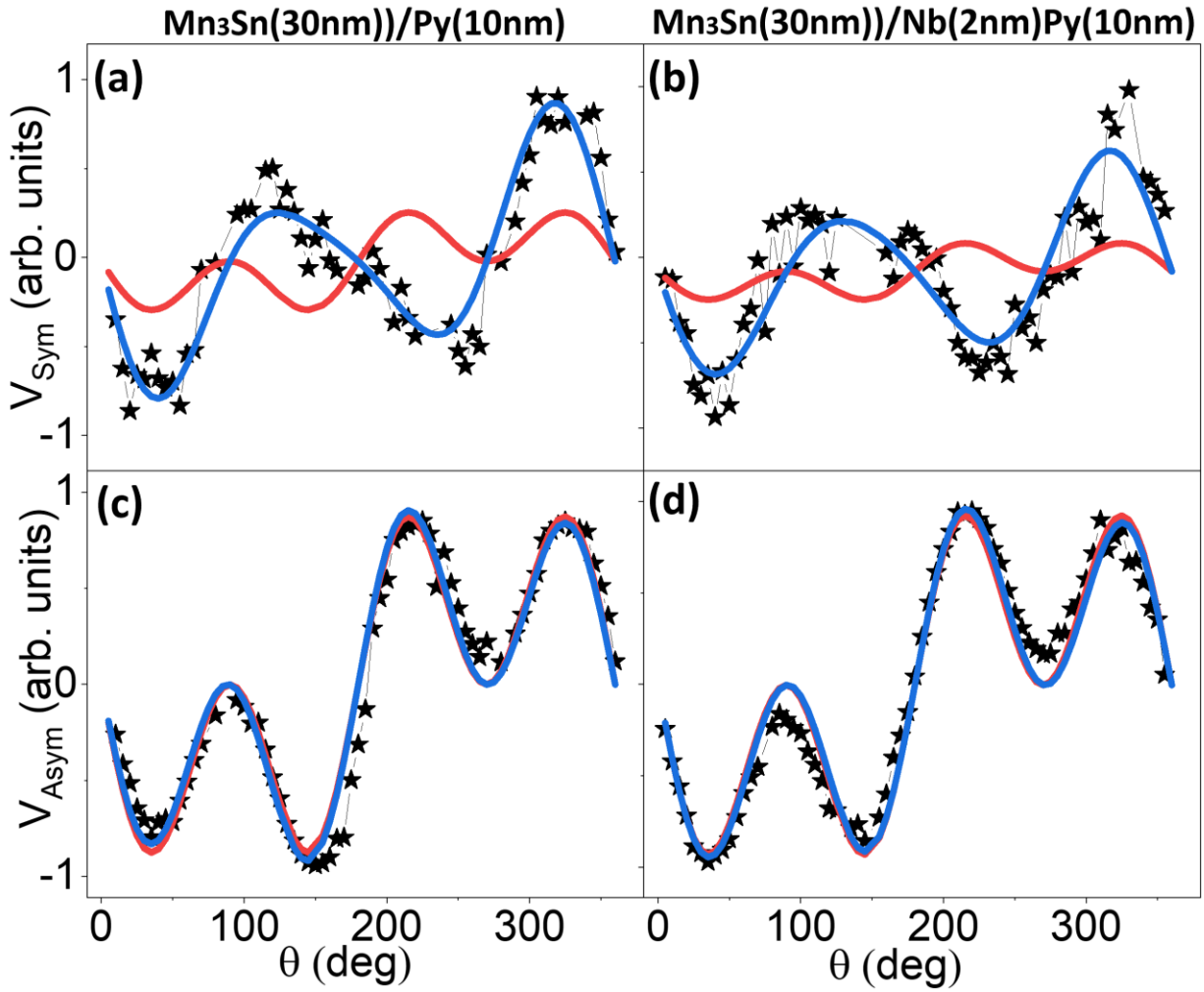

Figure 4 *Symmetric (a)(b) and antisymmetric (c)(d) rectifying voltages as a function of the in-plane external magnetic field angle θ from the current direction for Mn_3Sn(30nm)/Py(10nm) (left panel) and Mn_3Sn(30nm)/Nb(2nm)/Py(10nm) (right panel), respectively. The Blue curve is the fitting considering all τ^x, τ^y and τ^z and the red curve is the fitting only with τ^y*

DISCUSSION

It is well known that the V_{Asym} in ST-FMR, which measures out-of-plane torque, is dominated by the Oersted field contribution [14,26]. Therefore, the extracted τ_{FL}^{x}, τ_{FL}^{y} and τ_{DL}^{z} are not reliable. On the other hand, the extracted torques from MOKE measurements are much more accurate since the technique is less sensitive to heating and other nonlinear effects. Even more importantly, the Oersted field effect

contribution can be minimized in MOKE [13,16,27]. The ratio of in-plane torques τ_{DL}^{x}: τ_{DL}^{y} are consistent between ST-FMR and MOKE measurements. The magnitude τ_{DL}^{x} and τ_{FL}^{x} are about 30% of the conventional τ_{DL}^{y} and τ_{FL}^{y}, respectively, suggesting sizable spin polarization along the *x*-axis. In addition, τ_{DL}^{z} is also about 30% of τ_{FL}^{y}. τ_{DL}^{z} is particularly interest since it will lead to deterministic magnetization switching without a bias magnetic field for a perpendicular magnetization.

Theoretically, the spin orientation along *z*-axis has been predicted in Mn_3Sn when spin-orbit coupling (SOC) is considered [28]. However, those calculations did not produce spin polarization along *x*-axis. The discrepancy may arise from the fact that the theory only considers a single domain with current flowing along the octupole moment direction along *x*-axis. The generation of unusual spin orientation can be understood by spin rotation as we discussed in the introduction. Mn_3Sn behaves like a FM with octupole moment. The spin orientation in *y*-axis from conventional SHE will rotate around the octupole moment. For octupole along *x*-axis, spin orientation along *z*-axis will be generated. For an octupole moment away from the *x*-axis, spin polarization along *z*- and *x*-axes are both generated as illustrated in Figure 5. When the octupole moment is in y-direction, no rotation would occur, resulting in the absence of τ^{x} (Figure 3) and τ^{z}. Considering possible octupole moment orientation in Mn_3Sn [10], we therefore expect the observation of spin polarization along *x*-axis. In addition, there will be more electrons with spin orientation along z-axis than *x*-axis. It should also be noted that out-of-plane tilted octupole moment will also produce spin polarization along *x*-axis, which is actually theoretically predicted in Mn_3Ir whose octupole moment is tilted away from the in-plane direction [28].

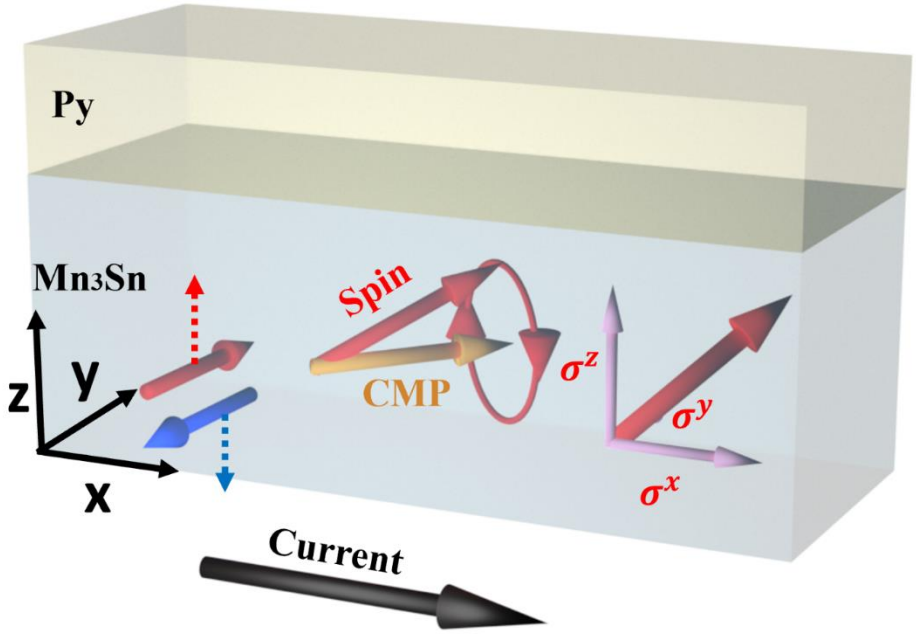

Figure 5 *By passing a current in the x-direction, the conventional SHE will create a spin polarization along the y-direction. In the presence of the octupole moment (CMP) in the xy-plane, the x-polarized spin orientation will precess around the octupole moment. This gives rise to a spin polarization with components along all three directions*

As both SHE and Rashba effect can produce spin-orbit torques and spin rotation [29–32] and it is challenging to truly separate these two effects. However, the Rashba effect is sensitively depending on the interface. Therefore, we inserted a thin Nb layer, which is a spin-transparent material with small SHA ($\theta_{SH} \approx -0.001$) [33], at the Mn_3Sn and NiFe interface. While the measured torques reduced in amplitude, the ratios of τ_{FL}^{x}: τ_{FL}^{y} and τ_{DL}^{x}: τ_{DL}^{y} remains the same (Table 1). This strongly indicates that spin-orbit torque in Mn_3Sn/NiFe is dominated by the bulk (SHE) effect.

In summary, we observed spin-orbit torque with unusual spin orientation in both *x*- and *z*-directions. The results are confirmed with both MOKE and ST-FMR measurements. The mechanism arises from non-collinear spin structure with spin-orbit coupling and it can be viewed as spin rotation around the octupole moment, the lowest order of cluster multipole moment pertaining to Mn_3Sn crystal group. We further demonstrate that the effect arises from the bulk SHE in Mn_3Sn. The study provides essential insight to better understanding how spin current with unusual spin orientation arises from the non-collinear AFM system.

Acknowledgement:

The work is supported by the National Science Foundation (NSF) under Award No. DMR1904076. The MOKE characterization is supported by NSF MRSEC under Award No. DMR-2011824 and is benefited from NSF Major Research Instrumentation under Award No. 1624976.

Reference:

[1] M. I. Dyakonov and V. I. Perel, *Current-Induced Spin Orientation of Electrons in Semiconductors*, Phys. Lett. A **35**, 459 (1971).

[2] J. Sinova, S. O. Valenzuela, J. Wunderlich, C. H. Back, and T. Jungwirth, *Spin Hall Effects*, Rev. Mod. Phys. **87**, 1213 (2015).

[3] D. MacNeill, G. M. Stiehl, M. H. D. Guimaraes, R. A. Buhrman, J. Park, and D. C. Ralph, *Control of Spin–Orbit Torques through Crystal Symmetry in WTe_2/Ferromagnet Bilayers*, Nature Physics **13**, 300 (2016).

[4] A. M. Humphries, T. Wang, E. R. J. Edwards, S. R. Allen, J. M. Shaw, H. T. Nembach, J. Q. Xiao, T. J. Silva, and X. Fan, *Observation of Spin-Orbit Effects with Spin Rotation Symmetry*, Nat. Commun. **8**, 911 (2017).

[5] S. Tomiyoshi, *Magnetic Structure and Weak Ferromagnetism of Mn_3Sn Studied by Polarized Neutron Diffraction*, J Physical Soc Japan **51**, 2478 (1982).

[6] P. J. Brown, V. Nunez, F. Tasset, J. B. Forsyth, and P. Radhakrishna, *Determination of the Magnetic Structure of Mn_3Sn Using Generalized Neutron Polarization Analysis*, Journal of Physics: Condensed Matter **2**, 9409 (1990).

[7] K. Kuroda, T. Tomita, M.-T. Suzuki, C. Bareille, A. A. Nugroho, P. Goswami, M. Ochi, M. Ikhlas, M. Nakayama, S. Akebi et al., *Evidence for Magnetic Weyl Fermions in a Correlated Metal*, Nature Materials **16**, 1090 (2017).

[8] N. P. Armitage, E. J. Mele, and A. Vishwanath, *Weyl and Dirac Semimetals in Three-Dimensional Solids*, Rev. Mod. Phys. **90**, 015001 (2018).

[9] M. Kimata, H. Chen, K. Kondou, S. Sugimoto, P. K. Muduli, M. Ikhlas, Y. Omori, T. Tomita, Allan. H. MacDonald, S. Nakatsuji and Y. Otani, *Magnetic and Magnetic Inverse Spin Hall Effects in a Non-Collinear Antiferromagnet*, Nature **565**, 627 (2019).

[10] M. T. Suzuki, T. Koretsune, M. Ochi, and R. Arita, *Cluster Multipole Theory for Anomalous Hall Effect in Antiferromagnets*, Phys. Rev. B **95**, 094406 (2017).

[11] S. Hu, D.-F. Shao, H. Yang, M. Tang, Y. Yang, W. Fan, S. Zhou, E. Y. Tsymbal, and X. Qiu, *Efficient Field-Free Perpendicular Magnetization Switching by a Magnetic Spin Hall Effect*, Nat. Commun. **13**, 4447 (2022).

[12] K. Kondou, H. Chen, T. Tomita, M. Ikhlas, T. Higo, A. H. MacDonald, S. Nakatsuji, and Y. C. Otani, *Giant Field-like Torque by the out-of-Plane Magnetic Spin Hall Effect in a Topological Antiferromagnet*, Nat. Commun. **12**, 6491 (2021).

[13] X. Fan, A. R. Mellnik, W. Wang, N. Reynolds, T. Wang, H. Celik, V. O. Lorenz, D. C. Ralph, and J. Q. Xiao, *All-Optical Vector Measurement of Spin-Orbit-Induced Torques Using Both Polar and Quadratic Magneto-Optic Kerr Effects*, Appl. Phys. Lett. **109**, 122406 (2016).

[14] L. Liu, T. Moriyama, D. C. Ralph, and R. A. Buhrman, *Spin-Torque Ferromagnetic Resonance Induced by the Spin Hall Effect*, Phys. Rev. Lett. **106**, 036601 (2011).

[15] Y. K. Kato, R. C. Myers, A. C. Gossard, and D. D. Awschalom, *Observation of the Spin Hall Effect in Semiconductors*, Science (1979) **306**, 5703 (2004).

[16] Z. Q. Qiu and S. D. Bader, *Surface Magneto-Optic Kerr Effect*, Review of Scientific Instruments **71**, 1243 (2000).

[17] D. Khadka, T.R. Thapaliya, S. Hurtado Parra, X. Han, J. Wen, R. F. Need, P. Khanal, W. Wang, J. Zang, J. M. Kikkawa, L. Wu and S. X. Huang, *Kondo Physics in Antiferromagnetic Weyl Semimetal $Mn_{3+x}Sn_{1-x}$ Films*, Sci. Adv. **6**, (2020).

[18] V. Baltz, A. Manchon, M. Tsoi, T. Moriyama, T. Ono, and Y. Tserkovnyak, *Antiferromagnetic Spintronics*, Rev. Mod. Phys. **90**, 015005 (2018).

[19] Y. S. Ou, X. Zhou, R. Barri, Y. Wang, S. Law, J. Q. Xiao, and M. F. Doty, *Development of a System for Low-Temperature Ultrafast Optical Study of Three-Dimensional Magnon and Spin Orbital Torque Dynamics*, Review of Scientific Instruments **91**, 033701 (2020).

[20] H. Yang, Y. Sun, Y. Zhang, W. J. Shi, S. S. P. Parkin, and B. Yan, *Topological Weyl Semimetals in the Chiral Antiferromagnetic Materials Mn_3Ge and Mn_3Sn*, New J Phys. **19**, 015008 (2017).

[21] H. Tsai, T. Higo, K. Kondou, T. Nomoto, A. Sakai, A. Kobayashi, T. Nakano, K. Yakushiji, R. Arita, S. Miwa et al., *Electrical Manipulation of a Topological Antiferromagnetic State*, Nature **580**, 608 (2020).

[22] See Supplemental Material at [URL Will Be Inserted by Publisher] for discussing of the in-plane crystal orientation and the CMP direction of Mn_3Sn films.

[23] A. Markou, J. M. Taylor, A. Kalache, P. Werner, S. S. P. Parkin, and C. Felser, *Noncollinear Antiferromagnetic Mn_3Sn Films*, Phys. Rev. Mater. **2**, 51001 (2018).

[24] S. DuttaGupta, A. Kurenkov, Oleg A. Tretiakov, G. Krishnaswamy, G. Sala, V. Krizakova, F. Maccherozzi, S. S. Dhesi, P. Gambardella, S. Fukami and H. Ohno, *Spin-Orbit Torque Switching of an Antiferromagnetic Metallic Heterostructure*, Nat. Commun. **11**, 5715 (2020).

[25] P. K. Muduli, T. Higo, T. Nishikawa, D. Qu, H. Isshiki, K. Kondou, D. Nishio-Hamane, S. Nakatsuji, and Y. Otani, *Evaluation of Spin Diffusion Length and Spin Hall Angle of the Antiferromagnetic Weyl Semimetal Mn_3Sn*, Phys. Rev. B **99**, 184425 (2019).

[26] T. Nan, C. X. Quintela, J. Irwin, G. Gurung, D. F. Shao, J. Gibbons, N. Campbell, K. Song, S. -Y. Choi, L. Guo, R. et al., *Controlling Spin Current Polarization through Non-Collinear Antiferromagnetism*, Nat. Commun. **11**, 4671 (2020).

[27] J. Shi, V. Lopez-Dominguez, F. Garesci, C. Wang, H. Almasi, M. Grayson, G. Finocchio, and P. Khalili Amiri, *Electrical Manipulation of the Magnetic Order in Antiferromagnetic PtMn Pillars*, Nat. Electron **3**, 92 (2020).

[28] J. Železný, Y. Zhang, C. Felser, and B. Yan, *Spin-Polarized Current in Noncollinear Antiferromagnets*, Phys. Rev. Lett. **119**, 187204 (2017).

[29] W. Wang, T. Wang, V. P. Amin, Y. Wang, A. Radhakrishnan, A. Davidson, S. R. Allen, T. J. Silva, H. Ohldag, D. Balzar et al., *Anomalous Spin–Orbit Torques in Magnetic Single-Layer Films*, Nature Nanotechnology **14**, 819 (2019).

[30] A. Davidson, V. P. Amin, W. S. Aljuaid, P. M. Haney, and X. Fan, *Perspectives of Electrically Generated Spin Currents in Ferromagnetic Materials*, Phys. Lett. A **384**, 126228 (2020).

[31] S. Emori, T. Nan, A. M. Belkessam, X. Wang, A. D. Matyushov, C. J. Babroski, Y. Gao, H. Lin, and N. X. Sun, *Interfacial Spin-Orbit Torque without Bulk Spin-Orbit Coupling*, Phys. Rev. B **93**, 180402(R) (2016).

[32] V. P. Amin, J. Zemen, and M. D. Stiles, *Interface-Generated Spin Currents*, Phys. Rev. Lett. **121**, 136805 (2018).

[33] K. R. Jeon, C. Ciccarelli, H. Kurebayashi, J. Wunderlich, L. F. Cohen, S. Komori, J. W. A. Robinson, and M. G. Blamire, *Spin-Pumping-Induced Inverse Spin Hall Effect in Nb/$Ni_{80}Fe_{20}$ Bilayers and Its Strong Decay Across the Superconducting Transition Temperature*, Phys. Rev. Appl. **10**, 014029 (2018).